

Magnetic and structural properties of Co_2MnSi based Heusler compound

S. J. Ahmed[†], C. Boyer[#], M. Niewczas^{†‡*}

[†] *Materials Science and Engineering, McMaster University, Hamilton, Ontario, Canada*

[#] *Canadian Neutron Beam Centre, Canadian Nuclear Laboratories, Chalk River, Ontario, Canada*

[‡] *Brockhouse Institute of Materials Research, McMaster University, Hamilton, Ontario.*

* *E-mail: niewczas@mcmaster.ca*

ABSTRACT

The influence of antisite disorder occupancies on the magnetic properties of the half-metallic Co_2MnSi compound was studied by experimental techniques and first-principles calculations. The neutron diffraction studies show almost equal amount of Mn and Co disorders of 6.5% and 7.6%, which was found to be in good agreement with density functional theory (DFT) calculations of the stable Co_2MnSi system with the corresponding disorders. DFT studies reveal that antiferromagnetic interactions introduced by Mn disorder lead to a reduction of the net magnetic moment. The results are discussed in conjunction with neutron diffraction and magnetization measurements. Magnetotransport measurements revealed a positive magnetoresistance for bulk Co_2MnSi , which decreases as temperature increases. A Curie temperature of ~ 1014 K was determined for the compound by high-temperature electrical resistivity and dilatometry measurements.

Keywords: Heusler compounds; Half-metallicity; Antisite disorder; Neutron diffraction; Density Functional Theory; Magnetic properties; Magnetoresistance.

1. Introduction

Half-metallicity has been a topic of tremendous scientific attention for the last three decades since the theoretical prediction of a 100 % spin polarization in the half-Heusler NiMnSb [1] and later, on the full-Heusler Co_2MnSn [2]. Recent progress on the phenomenon has been extended to systems like Weyl semimetal [3–5], Dirac half-metals [6–8], d^0 - d half-Heusler [9, 10], and also, perovskites [11–13]. Nevertheless, low Curie temperatures of these systems has kept their room temperature operation still out of reach. In contrast, the transition metal based full-Heusler compounds offer half-metallicity accompanied by high Curie temperatures, scalability of electronic properties, and negligible spin-orbit coupling [14–25]. A 100% spin polarization, however, has not been achieved experimentally. The discrepancy between the theoretical predictions and experimental results is mainly attributed to the presence of structural disorder and the finite temperature effects [22, 26–30]. The transition metal elements in these compounds tend to swap sites with each other what introduces new states in the minority spin gap destroying half-metallic properties. The spin disorder that occurs at finite temperatures is another cause

of the destruction of half-metallic properties.

Within the full-Heusler class, one of the most highly considered candidates for half-metallic ferromagnetism, the Co-Mn-Si based compound Co_2MnSi exhibits a large theoretical spin band gap of ~ 0.4 eV [31] and a high Curie temperature of ~ 985 K [32, 33] that are desired attributes of materials for spintronics. The theoretical and experimental work conducted on Co_2MnSi in the last two decades has focused on the analysis of structural and magnetic properties and their relation to spin polarization [14, 16, 22, 28, 34–43]. The highest reported value of spin polarization, $\sim 93\%$, was measured by ultraviolet-photoemission spectroscopy for bulk Co_2MnSi at room temperature [42]. For thin films, spin polarization up to 89% has been observed at low temperatures where the effect of spin's disorder is minimized [38]. Recently, Moges et al. [44] studied the relationship of spin disorder with the temperature in off-stoichiometric $\text{Co}_2\text{MnSi}_{0.84}$ thin films. The authors reported for this compound a transverse magnetoresistance ratio (TMR) of 1400% at 4.2 K, compared to 300% at room temperature.

Despite numerous investigations, some aspects of structure-property relationship in Co_2MnSi compound need to be better understood. One question concerns the structural disorder between Co and Mn sites, which influences the properties of the compound and determines the half-metallic behaviour. The site occupancy parameters for Co_2MnSi was studied by Ravel et al. [35] using the neutron diffraction and X-ray absorption fine structure (EXAFS) technique. The results of these authors pointed towards a similar disorder affinity of $\sim 8\text{-}14\%$ for both Co and Mn sites. On the contrary, a theoretical study by Picozzi et al. [28] reported a difference of disorder affinity more than twice with a findings that Co disorder occurs less likely. Although, the disagreement was suggested to be related to the computational parameters, there has not been any further attempts to address this problem.

There are also inconsistencies in the reported magnetic moment of Co_2MnSi compound. The neutron diffraction measurements report it in the range between $5.16\text{-}5.62 \mu_B/f.u.$ at room temperature [33, 35] and $5.07 \mu_B/f.u.$ at 4 K [32]. Ravel and co-workers [35] has recommended that the refinement of magnetic moment requires further investigation. A recent theoretical study by Pradines et al. [22] and the earlier work by Picozzi et al. [28] both suggested a reduction of the total magnetic moment in equilibrium conditions at 0 K, due to an antiferromagnetic interactions induced by Mn antisite disorder. These predictions have never been verified experimentally.

Another question concerns the transport properties of Co_2MnSi under magnetic field. The longitudinal magnetotransport studies of the bulk Co_2MnSi by Ritchie et al. [37] reported that the system shows no magnetoresistance in the field of up to 5.5 Tesla. This finding however contradicts with the small positive magnetoresistance that is usually exhibited by the other half-metallic systems Co_2FeSi [45], $\text{Fe}_{0.8}\text{Co}_{0.2}\text{Si}$ [46] and CrO_2 [47, 48].

In the present work, we investigate the effect of disorder on the magnetic moment in

Co₂MnSi half-metallic Heusler alloy. The neutron diffraction studies of the compound were conducted at 298 K, 100 K, and 4 K to retrieve the structural and magnetic parameters. First-principles calculations with defects were performed that validate the experimental observations and explained the correlation of the disorder occupancies and the magnetic moment. Temperature and field dependent transport properties were investigated to elucidate the role of charge transport in the magnetism of Co₂MnSi.

2. Experimental and computational details

Co₂MnSi alloy was prepared by arc-melting of the pure elements (Co (99.95%), Mn(99.98%) and Si(99.999%)) under argon atmosphere. To improve homogeneity, the ingot was remelted three times. The excess Mn was added to compensate for the evaporation loss of the element. The compound was then sealed in an evacuated silica tube, annealed at 800 °C for two weeks and subsequently quenched in mixture of ice and water to further improve the crystallinity. No mass loss was observed due to annealing. Phase purity was confirmed by X-ray powder diffraction using *PANalytical X'Pert Pro diffractometer* with Co K α_1 radiation. The refining of the diffraction data was performed using the full-profile Rietveld refinement implemented in the FullProf program [49–51]. The magnetic configurations were generated with representation analysis program SARAh [52].

Single crystals of Co₂MnSi alloy were grown using the RF heating Czochralski crystal growth method in an argon atmosphere. The pure elements were melted in an alumina crucible and the crystal was pulled using a tungsten wire seed with a constant pulling rate of 0.5 mm/min and 30 rpm rotation. The Laue diffraction revealed that the crystal has grown along $\langle 100 \rangle$.

The neutron diffraction studies of Co₂MnSi compound were performed at the Canadian Institute for Neutron Scattering in Chalk River on the C2 High Resolution Powder Diffractometer with a wavelength of 1.33Å. The neutron wavelength was calibrated using a Al₂O₃ sample as a standard. The diffraction data were collected on the 4 gram of the powdered polycrystalline Co₂MnSi sample, sealed in a thin-walled vanadium tube under argon atmosphere.

The single-crystal diffraction (SCD) was acquired using the *Bruker Smart Apex2 CCD* with Mo K α_1 radiation on a tiny crystal piece, sizing about 100 μ m. The MAX3D [53] software was used to visualize the reciprocal space that confirmed the crystallinity of the material. The crystal structure was solved and refined using the SHELXS and SHELXL [54] software packages.

The measurement of the magnetization hysteresis loops was performed on a polycrystalline sample with the Quantum Design MPMS SQUID magnetometer in the applied magnetic field up to ± 4 Tesla.

The electrical resistivity was measured on a single crystal sample of gauge dimensions 6.62 mm \times 1.6 mm \times 0.48 mm with the Keithley 2182A nanovoltmeter and 6221 current

source, attached to the Quantum Design PPMS system. A four-point method of measuring potential drop across the sample was used to determine the sample resistance. The sample was mounted on a platform with a spring-loaded, point-contact potential and current leads. The potential drop was measured in Delta mode as the average of 100 current reversals. Between 2 K and 298 K, the resistivity measurements were conducted using PPMS platform to control the sample temperature. Between 450 K and 1050 K, the measurements were performed in the resistance furnace inside the quartz tube under argon protective atmosphere. A separately developed ceramic holder with a pressure-loaded, point-contact potential and current leads was used in high temperature resistivity measurements. The temperature was controlled with the thermocouple located in the vicinity of the sample.

The dilatometry measurements were carried out on a push-rod dilatometer system on 33 mm long cylindrical single crystal sample with a non-uniform diameter of ~ 2 mm.

The first-principle calculations were carried using the density functional theory (DFT) implemented in the Vienna ab-initio simulation program (VASP) package [55, 56], with the generalized gradient approximation (GGA) exchange correlation functional [57], under the Projector Augmented Wave (PAW) [58] functions. To address the electron localization of 3d states of Co and Mn atoms, GGA+U method [59] was used to obtain the system equilibrium. Effective Hubbard parameter, U_{eff} of 1.92 eV for Co 3d and 1.62 eV for Mn 3d states was applied which was previously successfully used for Co_2MnSi [60]. The formation enthalpy parameters for the optimized structures were computed with the HSE06 hybrid functional that estimate the exchange interaction more efficiently [61]. The Brillouin zone for single elementary cell calculations was sampled using $6 \times 6 \times 6$ k-mesh. To study the effect of antisite disorder in Co_2MnSi , a $2 \times 2 \times 2$ supercell was generated and the k-mesh was adjusted accordingly to maintain the same k-point density.

3. Results

3.1. Single crystal diffraction (SCD)

Co_2MnSi crystallizes with the $L2_1$ type crystal structure within the space group $225 Fm\bar{3}m$. The Co, Mn, and Si atoms are situated in the Wyckoff position 8c ($3/4, 1/4, 1/4$), 4a (0,0,0) and 4b ($1/2, 1/2, 1/2$), respectively. The refined single crystal structural parameters are summarized in Table 1 and 2. The obtained crystal structure was found to be in good agreement with previously published results [32, 62–66] available in the inorganic crystal structure database (ICSD) [67]. Note that, the refined XRD-SCD parameters did not yield the information on the transition metal Co-Mn antisite disorder which is considered as one of the main reasons for the weakening of half-metallicity in Co_2MnSi compound [35]. The absence of the very well known disorders can be explained by the similar X-ray scattering power of Co and Mn. Consequently, disorders in the range of $\sim 10\%$ that was observed previously by Ravel et al. [35] are indistinguishable with XRD.

Table 1: Crystallographic data for Co₂MnSi single crystal obtained from refinement of X-ray diffraction data (Mo K_α radiation, 298K)

Refined composition	Mn Co ₂ Si
Space group	$Fm\bar{3}m$
Lattice constant (Å)	5.6585(4)
Volume (Å ³)	181.18(2)
$\rho_{calc}(g/cm^3)$	7.3642
Z	4
2 θ range	12.48 – 88.3
Index ranges	$-7 \leq h \leq 10, -10 \leq k \leq 11 -9 \leq l \leq 11$
Reflections collected	537
Independent reflections	58 [$R_{int} = 0.0168, R_{sigma}=0.0098$]
Data/restraints/parameters	58/0/4
Goodness-of-fit on $ F ^2$	1.185
Largest diff. peak/hole (e/Å ³)	0.72/ – 0.59
R indices [$I \geq 2\sigma(I)$]	R ₁ =0.0175 wR ₂ =0.0487

Table 2: Occupancy and isotropic displacement parameters for Co₂MnSi single crystal.

Atom	x	y	z	Site	Occupancy	U_{eq} (Å ²)
Co	3/4	3/4	1/4	8c	1.00008	0.00406(18)
Mn	1/2	1/2	0	4a	0.99984	0.00404(19)
Si	0	0	1/2	4b	0.99984	0.005(3)

3.2. Neutron powder diffraction

In contrast to X-ray, neutron beam offers coherent scattering lengths of 2.53 fm for Co and -3.73 fm for Mn, respectively. As a consequence, antisite disorder between Co and Mn atoms becomes distinguishable. The neutron diffraction data were collected at 4 K, 100 K, and 298 K in an effort to accurately refine the structure, the magnetic moments and observe their variation with decreasing temperature. One of the challenges in performing a precise refinement for Co_2MnSi is the lack of paramagnetic state diffraction data that makes it difficult to differentiate between the structural and magnetic reflections. An ideal approach would involve conducting a refinement on data collected above the Curie temperature to obtain structural information which can then be used successively for magnetic structure determination. However, the high Curie temperature of Co_2MnSi does not permit the data collection in the paramagnetic state. Furthermore, as discussed earlier, X-ray diffraction can not also successfully capture the Co-Mn disorder accurately which makes refinement more challenging.

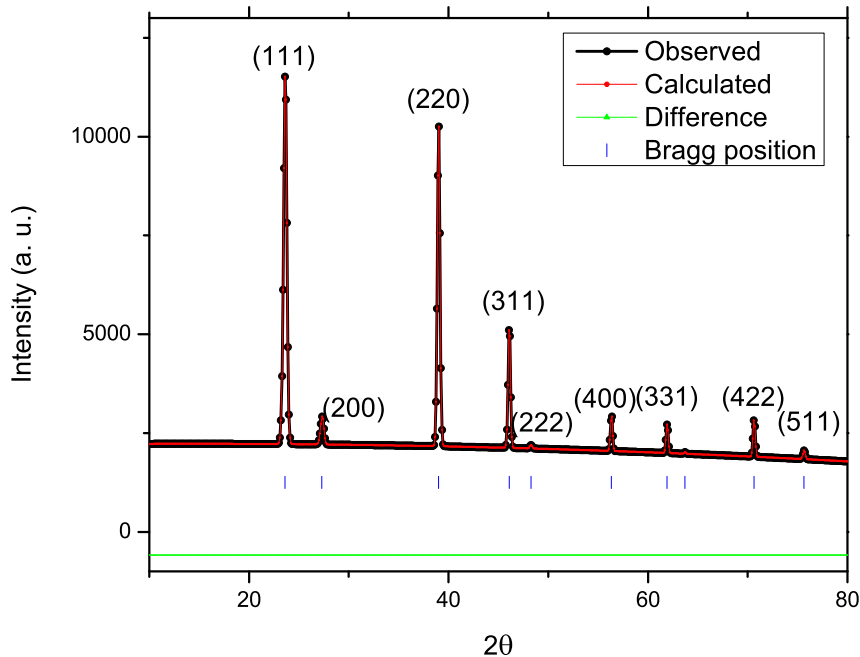


Fig. 1. Neutron pattern simulation of the magnetic structure with the parameters obtained from the first-principles calculation of defect free Co_2MnSi .

Simulation of magnetic reflections with the theoretically obtained magnetic moments (Fig. 1) suggest the presence of three dominant reflections (111), (220) and (311) for Co_2MnSi . Among these, the intensity of (111) and (310) are also significant to determine the Mn-Si disorder as they fall into the category with h, k, l all being odd [32]. As a

result, separating these magnetic reflections becomes crucial for a good refinement.

The pattern simulation in Fig. 1 shows that all the major magnetic peaks lie below the 2θ value of 46.5° . If the weak magnetic reflections above 46.5° are considered negligible, it can provide a means to obtain Co-Mn disorder more accurately. In this work, the structural refinement for Co_2MnSi was performed at higher angles within the range (47° - 117°). Such a refinement is feasible in the present case because in neutron scattering stronger reflections are observed at higher angles that allow proper identification of elements. The refinement profile is shown in Fig. 2a and refined structural parameters are listed in Table 3. It can be seen that Mn and Co tend to form antisite disorder among themselves with $\sim 6.5\%$ (3.25×2) Co sites being occupied by Mn and $\sim 7.6\%$ Mn sites being replaced by Co. Refinement involving a portion of Mn and Si sitting in each other's sites yielded almost negligible occupancy and was ignored in the subsequent refinement. The obtained occupancy parameters were kept constant and used in the successive magnetic refinements at 298 K, 100 K, and 4K. It should be noted that although the refinement ignored the presence of weaker magnetic reflections at higher angles, their presence in the refinement should be within the limit of experimental errors.

The magnetic structure at 298 K was refined with all structural parameters obtained from the higher angle refinement. The initial values of the magnetic moments were taken from our first-principles calculation that will be discussed in an upcoming section. The solution of the magnetic structure was based on the representation analysis approach using SARAh [52]. For the ordering, wave vector $\mathbf{k} = (0\ 0\ 0)$ was used since no extra magnetic reflection was observed. The method yielded only one basis vector, Γ_9 that corresponds to a ferromagnetic interaction. The final refined structural parameters are listed in Table 3, and the refinement profile is shown in Fig. 2(b). The refined ferromagnetic structure is displayed in Fig. 3. Obtained magnetic moment values of $2.432(37) \mu_B/f.u.$ for $4a$ site (Mn and Disorder Co) and $0.962(30) \mu_B/f.u.$ for $8c$ (Co and Disorder Mn) are much smaller compared to the previous results at 298 K [33, 35]. Note that, the neutron magnetic refinement was carried out for the particular magnetic sites rather than individual atoms. This is because the moments associated with disorder of $\sim 6.5\%$ and $\sim 7.6\%$ are usually small and can not be solved accurately using neutron diffraction technique. However, a site specific magnetic refinement captures the contribution from both the small antisite disorder and the parent occupant.

The refinement of the 100 K and 4 K neutron diffraction data were also performed with the occupancy parameters obtained from 298 K high angle structural refinement. No additional reflections were observed at low temperature revealing lack of any structural or magnetic transition below 100 K. The refinement profile is shown in Fig. 2(c) (100 K) and 2(d) (4 K), respectively. The relevant structural and magnetic parameter are listed in Table 3. The lattice constant of Co_2MnSi is less sensitive to the temperature, which is apparent when comparing their values at different temperatures. The magnetic moments are increased as the temperature is lowered. Nevertheless, the refined values at 4 K are much lower compared to the results of Webster [32] at the same temperature.

Table 3: Refined structural parameters for Co₂MnSi

Temperature	298 K-high angle	298 K	100 K	4 K
Spacegroup		Fm $\bar{3}$ m		
Lattice constant(\AA)	5.6406(4)	5.6406	5.6301(7)	5.6301(2)
Magnetic phase	-	Ferromagnetic		
Co and disorder Mn; and 8c (3/4, 3/4, 1/4)				
Occupancy (Co)		0.9675 (28)		
Occupancy (Mn)		0.0325 (28)		
B(\AA^2)	0.607(2)	0.607	0.4318(13)	0.3565(5)
M($\mu_B/f.u.$)	-	0.962(30)	1.008(16)	0.906(18)
Mn and Disorder Co; 4a (1/2, 1/2, 0)				
Occupancy (Mn)		0.924 (43)		
Occupancy (Co)		0.076 (43)		
B(\AA^2)	0.6877(1)	0.6877	0.4759(5)	0.5561(15)
M($\mu_B/f.u.$)	-	2.432(37)	2.456(32)	2.62(20)
Si; 4b (0, 0, 1/2)				
Occupancy (Si)		1		
B(\AA^2)	1.0177(14)	1.0177	1.1147(27)	1.1114(16)
χ^2	2.92	5.64	4.44	5.57
R_{wp}	14.5	13.6	13	13.1
R_F	4.38	4.58	6.16	6.23
R_{mag}	-	3.57	2.37	3.64

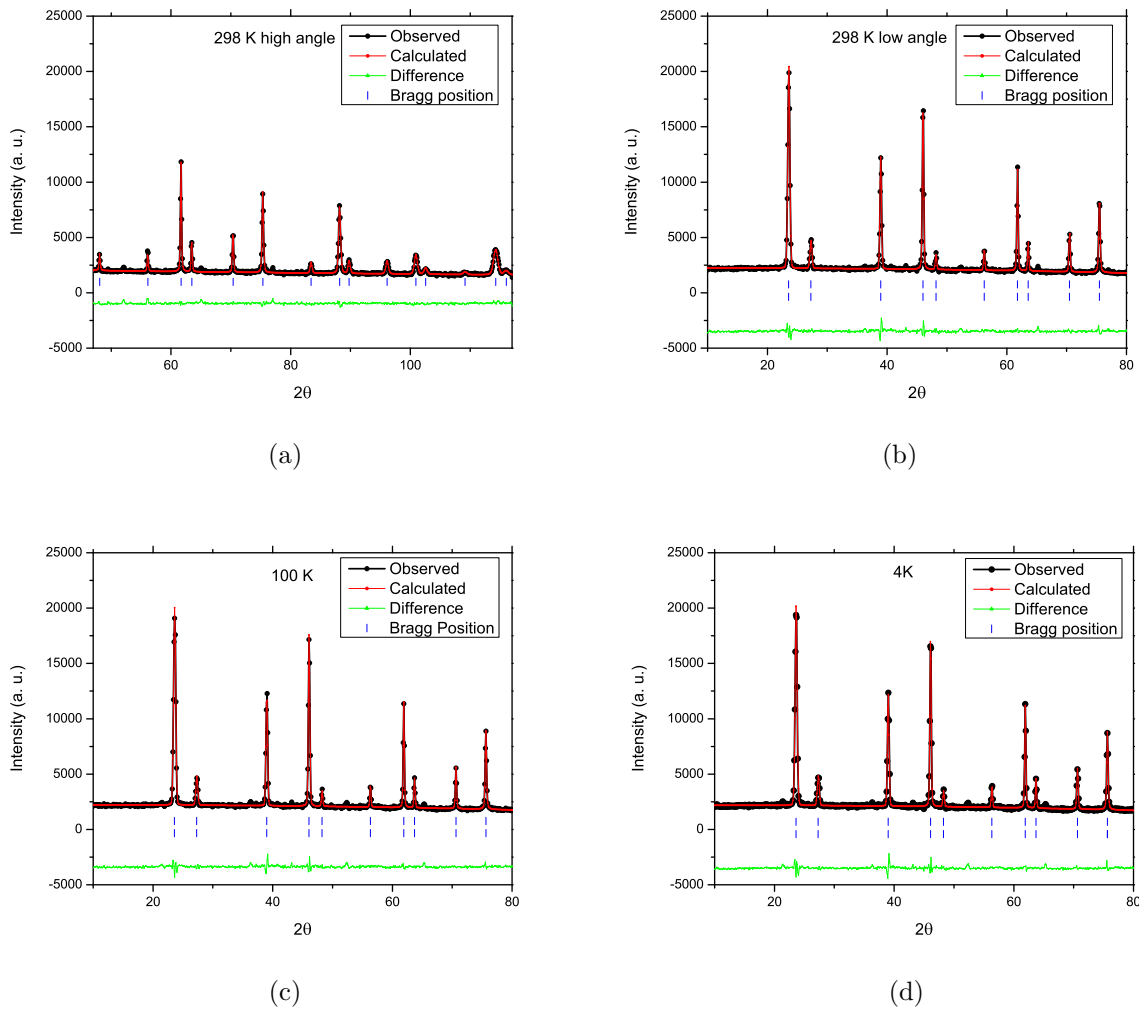


Fig. 2. Rietveld refinement profile of the neutron powder diffraction data at a) 298 K with high angle structural refinement, and b) 298 K c) 100 K and d) 4 K structural and magnetic refinement.

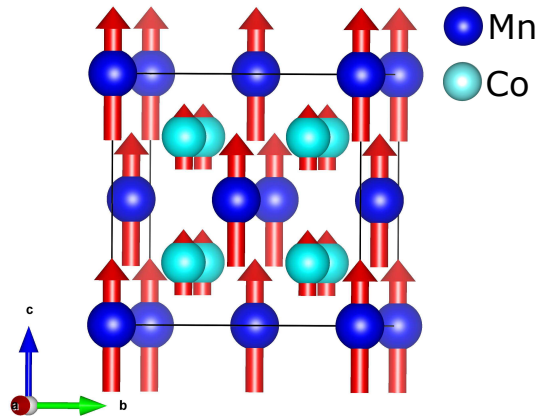


Fig. 3. Refined magnetic structure of Co_2MnSi of 298 K.

3.3. Magnetization behaviour

The hysteresis behaviour of the Co_2MnSi compound at 4 K, 100 K and 298 K is shown in Fig. 4. The compound exhibits almost identical saturation magnetization of (M_S) 4.94 (1), 4.99 (1) and 4.89 (1) $\mu_B/f.u.$ at 4 K, 100 K, and 298 K, respectively. Previous experimental measurements also reported comparable results of 4.96 $\mu_B/f.u.$ [33] and 5.15 $\mu_B/f.u.$ [35]. The coercive field was found to be ~ 20 (5) Oe for all the three temperatures of the study.

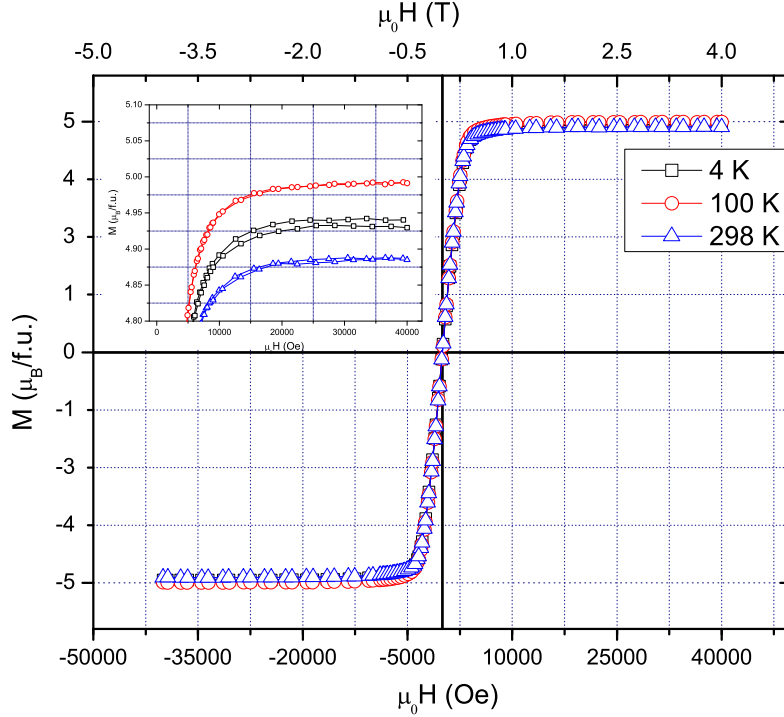


Fig. 4. Magnetic hysteresis loops at 4 K, 100 K and 298 K, measured with the applied field up to 40 kOe (4 Tesla). Inset shows the saturation magnetization at the corresponding temperatures.

3.4. Dilatometric measurements

The dilatometric measurements were performed on a single crystal sample to determine the Curie temperature. The technique has been used previously to determine the ferromagnetic to paramagnetic transition temperature of several compounds [68–71]. The change of length, ΔL and its derivative with respect to temperature, $\frac{d(\Delta L)}{dT}$, as a function of temperature for Co_2MnSi is shown in the Fig. 5. It can be seen that the length change starts to deviate from a linear responsive behaviour at higher temperatures where the ferromagnetic to paramagnetic phase transition takes place. From the sharp peak in the $\frac{d(\Delta L)}{dT}$, the Curie temperature was identified to be 1017 (3) K which compares well with the previously published T_C of 985 K [32, 33]

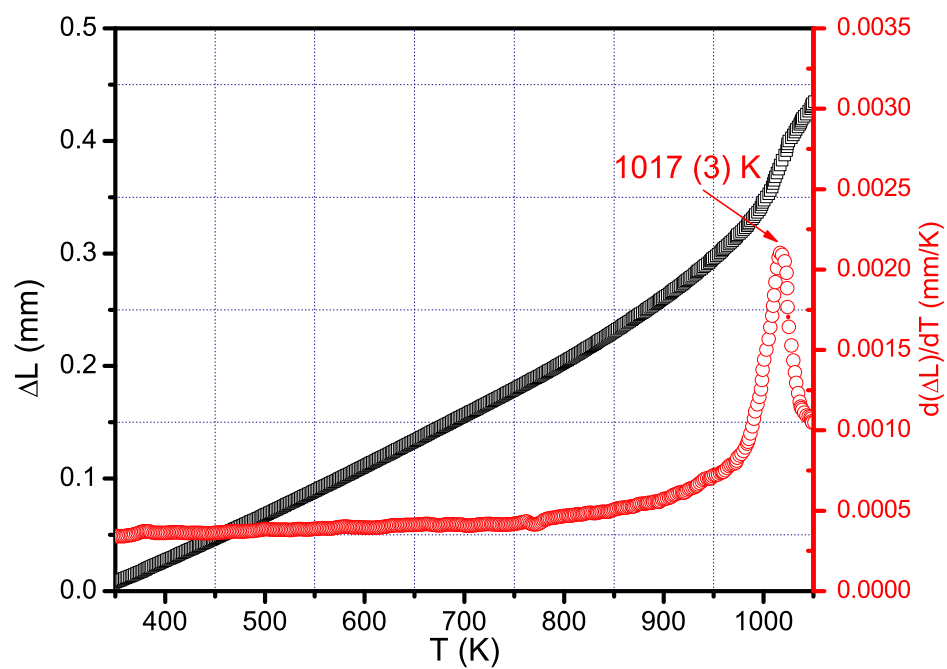


Fig. 5. ΔL and $\frac{d(\Delta L)}{dT}$ as a function temperature measured from 350 K to 1150 K. ΔL shows a linear response with temperature until near the magnetic phase transition point where the response changes. The Curie temperature was identified to be 1017 (3) K from the sharp peak in the $\frac{d(\Delta L)}{dT}$ vs T plot.

3.5. Transport properties

The total electrical resistivity of Co_2MnSi compound consists of three main contributions, the residual resistivity (ρ_R), magnonic (ρ_M) and phononic parts (ρ_P), as per Eq.1 [45].

$$\rho = \rho_R + \rho_M(T) + \rho_P(T). \quad (1)$$

The residual resistivity, ρ_R , is determined by the imperfections in the crystal. The magnetic resistivity, ρ_M , takes into account the exponential suppression of the quadratic temperature dependence due to magnon scattering [45, 72–74] and is given by (Eq.2):

$$\rho_M(T) = AT^2 e^{-\frac{\Delta}{T}}. \quad (2)$$

here, the constant A indicates the strength of magnon scattering and Δ is the minority spin gap at the Fermi level, E_F .

The phononic part of the electrical resistivity, ρ_P , is analyzed by the Bloch-Grüneisen formula (Eq.3).

$$\rho_P(T) = C \left(\frac{T}{\theta_D}\right)^n \int_0^{\frac{\theta_D}{T}} \frac{x^n}{(e^x - 1)(1 - e^{-x})} \quad (3)$$

where A is constant and θ_D is Debye temperature. A θ_D value of 520 K was reported for Co_2MnSi by Ito et al. [75]. The parameter n can be either 3 or 5 that identifies mechanism of phononic scattering. A fitting with $n = 3$ indicates an interband electron scattering from conduction band, while $n = 5$ corresponds to a intraband scattering.

For Co_2MnSi , the best fitting was obtained using $n = 3$ in the Bloch-Grüneisen expression (Eq. 3), as it is shown in Fig. 6(a). The residual resistivity, ρ_R was determined to be 4.5517 (10) $\mu\Omega\text{.cm}$, which is in good agreement with previously published values of 2 $\mu\Omega\text{cm}$ [36] and 7 $\mu\Omega\text{cm}$ [37]. It can be seen from the fitting parameters that electrical resistivity from 2 K to 300 K is completely dominated by the interband phonon scattering. The significantly small value 1.56 (2457) $\times 10^{-9}$ $\mu\Omega\text{.cm/K}^2$ of parameter A with higher errors indicates the magnon scattering to be almost negligible upto 300 K which also makes the obtained Δ of 305 (87) K unreliable. A temperature independent behavior was observed below 30 K, indicating the system to be a good metal at low temperatures. The residual resistivity ratio (RRR) at 300 K, i.e., the ratio of the resistance of the sample at 300 K over the resistance at 2 K, was found to be 3.5.

The Curie temperature was determined from the high temperature resistivity measurement with an apparent sudden change in the electrical resistivity at higher temperatures (Fig. 6(b)). From the peak of the $\frac{d(\rho)}{dT}$ vs. T plot, the Curie temperature was identified to be 1014 K which corresponds well to the dilatometry measurements. The RRR value for Co_2MnSi reaches ~ 50 near the transition temperature.

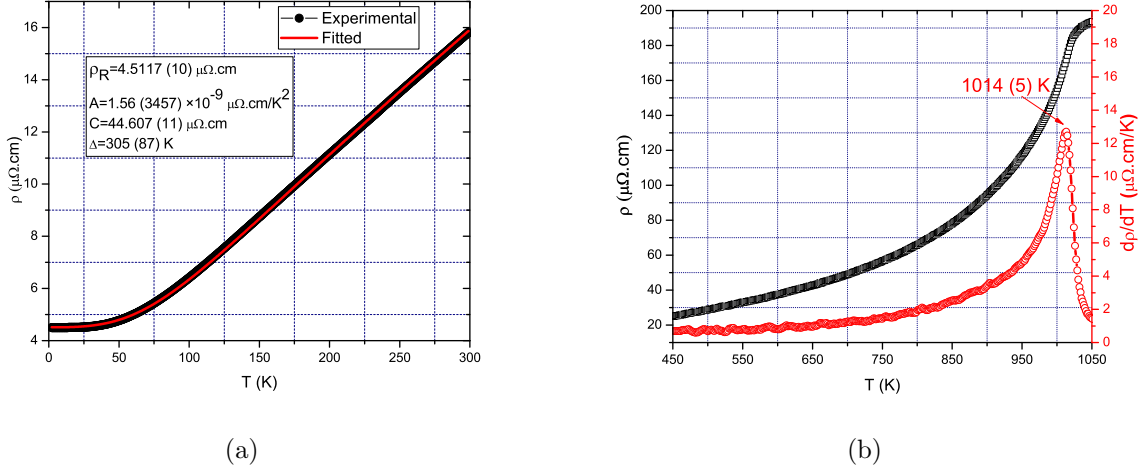


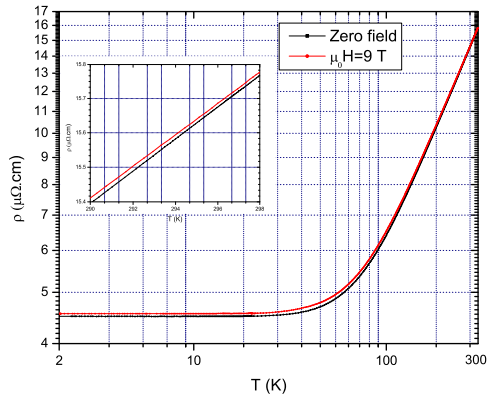
Fig. 6. a) Low temperature (2 K to 300 K) electrical resistivity of Co_2MnSi single crystal fitted using Eq. 1. High temperature electrical resistivity, ρ and $\frac{d\rho}{dT}$, as a function of temperature measured from 450 K to 1150 K. The Curie temperature was determined to be 1014 (5) K from the sharp change in the temperature dependence of $\frac{d\rho}{dT}$.

3.6. Magnetoresistance

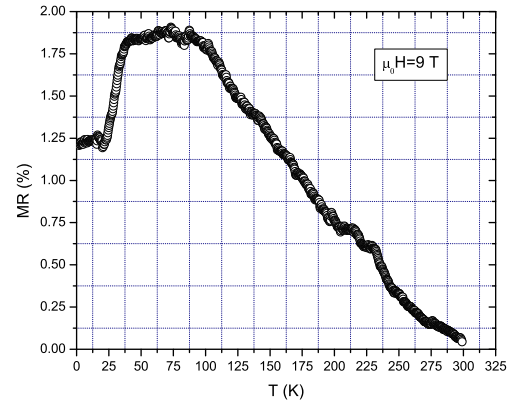
The magnetotransport of Co_2MnSi compound was measured between 2 K and 302 K, in the constant magnetic field of 9 Tesla applied perpendicular to the direction of current flow (transverse magnetoresistance). In comparison with the zero field data, Co_2MnSi shows a very small and positive increase in magnetoresistance up to room temperature (Fig. 7(a)). The magnetoresistance, $\text{MR} (\%) = \frac{\rho(9T) - \rho(0T)}{\rho(0T)} \times 100$, as a function of temperature ((Fig. 7(b))) shows a maximum value of 1.88(1)% at 68 K, which decreases to 0.06(1)% at 300 K. Fig. 7(c) shows the field dependence of the electrical resistivity at 2 K. The resistance of Co_2MnSi increases roughly parabolically with the applied field, with the value of $\text{MR} \sim 1.22(1)\%$ at the highest field of 9 Tesla available in our system (Fig. 7(c)).

3.7. First-principle calculations

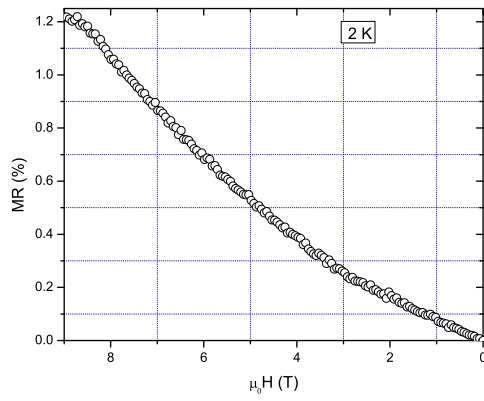
Calculations were carried out on a pure Co_2MnSi , as well as the structures with different concentrations of disorder that are relevant to the experimental observations. Before computation of the energy, a complete first-principles structural relaxation was performed. Here, we consider various Co-Mn antisite disorders and discuss their propensity to form in terms of the energy difference with the ideal Co_2MnSi . Note that these calculations do not include any disorder involving the Si (4b) site as they have not been observed in any previous experimental investigations [32, 33, 35], nor in the present work. Four different types of defects were studied with all the calculations done with a 128 atoms unit cell. The first one considers a Mn only antisite disorder created by replacing one Co atom to obtain a $(\text{Co}_{0.984}\text{Mn}_{0.016})_2\text{MnSi}$ stoichiometry. The second one corresponds to a Co only antisite with a composition of $(\text{Co}_2(\text{Mn}_{0.969}\text{Co}_{0.031})\text{Si})$. The third and fourth type



(a)



(b)



(c)

Fig. 7. a) Temperature dependence of electrical resistivity in a zero (black) and 9 Tesla magnetic field (red), showing a very small increase in electrical resistivity under the external field. Inset shows the comparison of the data near room temperature. b) Change in magnetoresistance, MR (%), as a function of temperature. c) Magnetoresistance at 2 K as a function of magnetic field measured from the saturated state at 9 Tesla down to 0 Tesla.

of defects involves disorder between both Co-Mn at concentrations that are relevant to the experimental results. It should be noted that the neutron refinement in this study and other experimental investigations indicated slightly different disorder affinity for the Mn and Co sites. In the first-principle calculations, however, we adjusted the identical disorder occupancy between Co and Mn to preserve accurate stoichiometry. The computed energies are listed in Table 4. The computed defect formation energies included the addition and subtraction of the excess pure Co and Mn from the reservoirs.

Table 4: Defect formation energies for the disordered configurations in the 128 atoms supercell Co_2MnSi . The energy for the ideal structure without any defect is taken as 0.

Type of disorder	Composition	Required energy (eV/f.u.)
Defect free	Co_2MnSi	0
Only Mn antisite	$(\text{Co}_{0.984}\text{Mn}_{0.016})_2\text{MnSi}$	0.041
Only Co antisite	$(\text{Co}_2(\text{Mn}_{0.969}\text{Co}_{0.031})\text{Si})$	0.30
Co-Mn swap	$(\text{Co}_{0.969}\text{Mn}_{0.031})_2(\text{Mn}_{0.938}\text{Co}_{0.062})\text{Si}$	0.015
Co-Mn swap	$(\text{Co}_{0.953}\text{Mn}_{0.047})_2(\text{Mn}_{0.906}\text{Co}_{0.094})\text{Si}$	0.073

From Table 4, it can be seen that formation of a single Mn antisite defect (1.6%) in Co_2MnSi requires external energy of 0.041 eV/f.u while the single Co counterpart (3.1%) requires 0.3 eV/f.u. The calculation is consistent with the work of Picozzi et al. [28], which showed the Co only antisite disorder is energetically less favourable. Formation of such single antisite defects requires, however, an excess supply of Mn/Co from the reservoir and expelling of an equivalent concentration Co/Mn from the ideal structure that break the ideal 2:1:1 stoichiometry. In comparison, as can be seen in Table 4, equivalent Mn-Co antisite disorders with higher defect concentrations requires much less energies. In our calculations, the formation of 6.2% and 9.4% antisite Co-Mn disorder was requires 0.015 eV/f.u. and 0.073 eV/f.u, respectively. These correspond to thermal energies at 173 K and 846 K, which are usually encountered during the experiments. Furthermore, these equivalent Co-Mn swaps maintains the ideal 2:1:1 stoichiometry and thus are more favourable to form, in contrast to the Mn or Co only antisite disorder. Note that our computed energies are in good agreement with the reported energies by Pradines et al. [22] with similar defect concentrations.

In the next step, we considered the effect of defect concentrations on the magnetic properties of Co_2MnSi . Here, the ideal Co_2MnSi was compared with the structure containing 6.2% and 9.4% Co-Mn antisite disorder, discussed above. The magnetic moments are listed in Table 5. From Table 5, it is evident that the net magnetic moment is significantly reduced with the introduction of the antisite disorder. This suppression is caused by an antiferromagnetic interactions of the Mn antisite disorder with the parent Mn atoms, which was also reported in previous theoretical examinations [22, 28]. The emergence of these interactions can be attributed to the reduction of Mn-Mn interatomic distances due to the disordered Mn replacing Co atoms in the 8c site [22]. In the previous

Table 5: Average magnetic moment from the first-principle calculations. Column "A" stands for the $(\text{Co}_{0.969}\text{Mn}_{0.031})_2(\text{Mn}_{0.938}\text{Co}_{0.062})\text{Si}$ composition. Column "B" describes $(\text{Co}_{0.953}\text{Mn}_{0.047})_2(\text{Mn}_{0.906}\text{Co}_{0.094})\text{Si}$ compound.

Atom	Site	Magnetic Moment ($\mu_B/f.u.$)		
		Co ₂ MnSi	A	B
Co	8c	0.974	1.138	1.114
Mn disorder	8c	-	-0.111	-0.164
Mn	4a	3.49	2.666	2.558
Co disorder	4a	-	0.139	0.18
Si	4b	-0.102	-0.072	-0.069
Interstitial region		-0.298	-0.256	-0.257
Net moment		5.04	4.533	4.311

studies by Pradines et al. [22], it was found that introduction of 6.2% disorder reduces the average magnetic moment of Mn atoms in the 4a to $2.667 \mu_B/f.u.$ with some Mn atoms coupling antiferromagnetically with the disorder Mn in 8c. As the concentration of disorder increases, more Mn atoms occupy the 8c sites. Consequently, it is expected that antiferromagnetic interaction will be stronger and the reduction of both Mn and hence the total magnetic moment will be higher, which is reflected in the values for 9.4% Co-Mn swap.

4. Discussion

4.1. Occupancy of Co and Mn antisite disorder

The neutron diffraction data were collected on a polycrystalline sample that was water quenched from 1073 K (800°C) to freeze the state of the system at that temperature. The refinement of the data reveal that the occupancies of the Mn and Co antisite disorder in the state at 1073 K are $\sim 6.5\%$ and $\sim 7.6\%$, respectively (Table 3). In contrast, the first-principles calculation showed that the formation of 6.2% and 9.4% equivalent Co-Mn disorder requires temperature of 173 K and 846 K, respectively. The disagreement between the theoretical and experimental observations can be attributed to several experimental and theoretical error factors. Some imbalance can originate from the smaller lattice constant obtained theoretically, which in turn produces slightly lower energy compared to the energy that would be obtained with experimentally synthesized structures [22]. Additionally, an error may also be introduced by the experimentally refined antisite disorder with dissimilar amounts of Co and Mn. In contrast, our first-principles calculations suggest the formation of disorder with identical Co and Mn concentrations is more favorable. Other experimental error factors that are difficult to control are related to: (i) the contribution from weak magnetic reflections at higher 2θ angle data, (ii) evaporation of Mn during arc melting, which is a common problem in synthesis of Mn based compounds, (iii) purity of the elements used to produce Co₂MnSi, (iv) the exact quenching temperature being less than 800°C due to the evacuated quartz tube. All these factors can contribute

to the observed slight difference in the theoretical and experimental disorder occupancy. Nonetheless, disorder of 9.4% at 846 K calculated from the first principles and the disorder of $\sim 6.5-7.6\%$ obtained from the neutron refinement of sample annealed at 1073 K can be regarded to be in fair agreement with each other.

4.2. Influence of disorder on magnetic properties

The first principle calculations predict a total magnetic moment of $4.53 \mu_B/f.u.$ for 6.2% disorder and of $4.31 \mu_B/f.u.$ for 9.4% disorder, compared to a moment of $5.04 \mu_B/f.u.$ for defect-free structure. Such suppression of the magnetic moment with the increasing degree of disorder arises from the antiferromagnetic interactions between Mn atoms that decrease their moment. The influence of the antiferromagnetic Mn atoms is also reflected in the neutron diffraction refinement with a total moment of ~ 4.356 at 298 K, $4.472 \mu_B/f.u.$ at 100 K and 4.432 at 4 K $\mu_B/f.u.$. The magnetic moments for the 8c site that contains Co and disordered Mn were found to be $0.906(18) \mu_B/f.u.$ at 4 K. In contrast, the first-principles calculation that corresponds to a 0 K condition yielded moments of $1.027 \mu_B/f.u.$ (1.138-0.111) and $0.95 \mu_B/f.u.$ (1.114-0.164) for the 6.2% and 9.4% disordered 8c site, respectively. These results are considered to be in excellent agreement with the experimental observation. The refined moments for the 4a sites at 4 K from neutron diffraction were found to be $2.62(20) \mu_B/f.u.$, which is also in good agreement with the theoretically obtained $2.805 \mu_B/f.u.$ ($2.666+0.139$) for 6.2% disorder and $2.738 \mu_B/f.u.$ ($2.555+0.18$) for 9.4% disorder.

The measurements of the magnetization hysteresis show a saturation magnetization of 4.94 (1), 4.99 (1) and 4.89 (1) $\mu_B/f.u.$ at 298 K, 100 K and 4 K, respectively. These figures are very close to the theoretically predicted value of the total moment for defect-free compound, $5.04 \mu_B/f.u.$, where all atomic moments are ferromagnetically aligned in the applied field of 4 Tesla. Such results are not surprising as they indicate that the antiferromagnetic interactions between the Mn atoms are relatively weak in nature.

4.3. Magnetotransport

Due to the negligible magnon scattering, an accurate determination of the energy gap parameter Δ , from the fitting the temperature dependent resistivity data in Fig. 6(a), was not possible. Nevertheless, the presence of a near zero positive magnetoresistance at 298 K (Fig. 7(a)), indicates the Δ is close to room temperature. An exponential decrease of the electron magnon scattering is expected for a half-metallic system with one spin state [45]. Very small value of A constant obtained from the resistivity fitting in Fig. 6(a) indicates that electron magnon scattering is becoming weaker as the temperature decreases and vanishes above 298 K. The presence of an exponential factor is indeed visible in the high-temperature resistivity data in Fig. 6(b). The positive magnetoresistance in the system is dominated by the conventional cyclotron effect and the scattering of the electrons on phonons and impurities [76]. Note that, the absence of magnetoresistance in the study of Ritchie et al. [37] is likely due to the longitudinal magnetoresistance being much weaker in the magnitude than the transverse magnetoresistance measured here.

5. Conclusions

We performed an experimental and theoretical study of the structural disorder and its influence on the magnetic properties in the half-metallic Co_2MnSi compound. The results suggest that the system consists of equivalent concentrations of disorders involving Co and Mn sites. From the neutron diffraction studies, the Co and Mn disorder of $\sim 6.5\%$ and $\sim 7.6\%$ was obtained, which was corroborated by the theoretical study. The results indicate that the antisite disorder is unavoidable in Co_2MnSi since the formation of such disorder is energetically favorable in ambient conditions. Antiferromagnetic interactions due to disordered Mn atoms were detected by the first-principles calculations and were correlated with a reduction of the magnetic moments obtained from the refinement of neutron diffraction data at 298 K, 100 K, and 4 K. Co_2MnSi compound shows positive magnetoresistance, which decreases as temperature increases to room temperature. The system exhibits a ferromagnetic to paramagnetic transition at ~ 1014 K, which was determined by the high-temperature dilatometry and electrical resistivity measurements.

Acknowledgements

The authors thank Dr. O. Rubel for the help with first-principles calculations. Financial support of Natural Sciences and Engineering Research Council of Canada under the NSERC Discovery Grant: "Artificially Structured Multiferroic Composites based on the Heusler alloys" is gratefully acknowledged.

References

- [1] R. De Groot, F. Mueller, P. Van Engen, K. Buschow, New class of materials: half-metallic ferromagnets, *Phys. Rev. Lett.* 50 (1983) 2024.
- [2] J. Kübler, A. William, C. Sommers, Formation and coupling of magnetic moments in heusler alloys, *Phys. Rev. B* 28 (1983) 1745.
- [3] Q. Xu, E. Liu, W. Shi, L. Muechler, J. Gayles, C. Felser, Y. Sun, Topological surface fermi arcs in the magnetic weyl semimetal $\text{Co}_3\text{Sn}_2\text{S}_2$, *Phys. Rev. B* 97 (2018) 235416.
- [4] E. Liu, Y. Sun, N. Kumar, L. Muechler, A. Sun, L. Jiao, S.-Y. Yang, D. Liu, A. Liang, Q. Xu, et al., Giant anomalous hall effect in a ferromagnetic kagome-lattice semimetal, *Nat. Phys.* (2018) 1.
- [5] Q. Wang, Y. Xu, R. Lou, Z. Liu, M. Li, Y. Huang, D. Shen, H. Weng, S. Wang, H. Lei, Large intrinsic anomalous hall effect in half-metallic ferromagnet $\text{Co}_3\text{Sn}_2\text{S}_2$ with magnetic weyl fermions, *Nat. Commun.* 9 (2018) 3681.
- [6] Q. Sun, N. Kioussis, Prediction of manganese trihalides as two-dimensional dirac half-metals, *Phys. Rev. B* 97 (2018) 094408.

- [7] F. Ma, Y. Jiao, Z. Jiang, A. Du, Rhombohedral lanthanum manganite: a new class of dirac half-metal with promising potential in spintronics, *ACS Appl. Mater. Interfaces* 10 (2018) 36088–36093.
- [8] Y.-p. Wang, S.-s. Li, C.-w. Zhang, S.-f. Zhang, W.-x. Ji, P. Li, P.-j. Wang, High-temperature dirac half-metal PdCl_3 : a promising candidate for realizing quantum anomalous hall effect, *J. Mater. Chem. C* 6 (2018) 10284–10291.
- [9] S. Davatolhagh, A. Dehghan, Dirac-like half-metallicity of d0- d half-heusler alloys, *Phys. C.* (2018).
- [10] A. Dehghan, S. Davatolhagh, d0-d half-heusler alloys: A potential class of advanced spintronic materials, *J. Alloys Compd.* 772 (2019) 132–139.
- [11] N. Kim, R. Kim, J. Yu, Half-metallic ferromagnetism and metal–insulator transition in sn-doped SrRuO_3 perovskite oxides, *J. Magn. Magn. Mater.* 460 (2018) 54–60.
- [12] H. Hsu, S.-C. Huang, Simultaneous metal–half-metal and spin transition in SrCoO_3 under compression, *Phys. Rev. Mater.* 2 (2018) 111401.
- [13] N. Zu, R. Li, R. Ai, Structural, electronic and magnetic properties and pressure-induced half metallicity in double perovskite Ca_2AOSO_6 (a= cr, mo), *J. Magn. Magn. Mater.* 467 (2018) 145–149.
- [14] S. Ishida, S. Fujii, S. Kashiwagi, S. Asano, Search for half-metallic compounds in Co_2MnZ (z= iib, ivb, vb element), *J. Phys. Soc. Jpn.* 64 (1995) 2152–2157.
- [15] K. Inomata, S. Okamura, R. Goto, N. Tezuka, Large tunneling magnetoresistance at room temperature using a heusler alloy with the b2 structure, *Jpn. J. Appl. Phys* 42 (2003) L419.
- [16] S. Kämmerer, A. Thomas, A. Hütten, G. Reiss, Co_2MnSi heusler alloy as magnetic electrodes in magnetic tunnel junctions, *Appl. Phys. Lett.* 85 (2004) 79–81.
- [17] K. Yakushiji, K. Saito, S. Mitani, K. Takanashi, Y. Takahashi, K. Hono, Current-perpendicular-to-plane magnetoresistance in epitaxial $\text{Co}_2\text{MnSi}/\text{Cr}/\text{Co}_2\text{MnSi}$ trilayers, *Appl. Phys. Lett.* 88 (2006) 222504.
- [18] T. Furubayashi, K. Kodama, H. Sukegawa, Y. Takahashi, K. Inomata, K. Hono, Current-perpendicular-to-plane giant magnetoresistance in spin-valve structures using epitaxial $\text{Co}_2\text{FeAl}_{0.5}\text{Si}_{0.5}/\text{Ag}/\text{Co}_2\text{FeAl}_{0.5}\text{Si}_{0.5}$ trilayers, *Appl. Phys. Lett.* 93 (2008) 122507.
- [19] K. Kodama, T. Furubayashi, H. Sukegawa, T. Nakatani, K. Inomata, K. Hono, Current-perpendicular-to-plane giant magnetoresistance of a spin valve using Co_2MnSi heusler alloy electrodes, *J. Appl. Phys.* 105 (2009) 07E905.

- [20] K. Nikolaev, P. Kolbo, T. Pokhil, X. Peng, Y. Chen, T. Ambrose, O. Mryasov, all-heusler alloy current-perpendicular-to-plane giant magnetoresistance, *Appl. Phys. Lett.* 94 (2009) 222501.
- [21] T. Graf, C. Felser, S. S. Parkin, Simple rules for the understanding of heusler compounds, *Prog. Solid State Chem.* 39 (2011) 1–50.
- [22] B. Pradines, R. Arras, I. Abdallah, N. Biziere, L. Calmels, First-principles calculation of the effects of partial alloy disorder on the static and dynamic magnetic properties of Co_2MnSi , *Phys. Rev. B* 95 (2017) 094425.
- [23] X. Wang, Z. Cheng, Y. Jin, Y. Wu, X. Dai, G. Liu, Magneto-electronic properties and tetragonal deformation of rare-earth-element-based quaternary heusler half-metals: A first-principles prediction, *J. Alloys Compd.* 734 (2018) 329–341.
- [24] J.-X. Wang, Z. Chen, Y. Gao, Phase stability, magnetic, electronic, half-metallic and mechanical properties of a new equiatomic quaternary heusler compound ZrRuTiIn : A first-principles investigation, *J. Phys. Chem. Solids* 116 (2018) 72–78.
- [25] L. Siakeng, G. M. Mikhailov, D. Rai, Electronic, elastic and x-ray spectroscopic properties of direct and inverse full heusler compounds Co_2FeAl and Fe_2CoAl , promising materials for spintronic applications: a dft+ u approach, *J. Mater. Chem. C* 6 (2018) 10341–10349.
- [26] A. MacDonald, T. Jungwirth, M. Kasner, Temperature dependence of itinerant electron junction magnetoresistance, *Phys. Rev. Lett.* 81 (1998) 705.
- [27] P. A. Dowben, R. Skomski, Finite-temperature spin polarization in half-metallic ferromagnets, *J. Appl. Phys.* 93 (2003) 7948–7950.
- [28] S. Picozzi, A. Continenza, A. J. Freeman, Role of structural defects on the half-metallic character of Co_2MnGe and Co_2MnSi heusler alloys, *Phys. Rev. B* 69 (2004) 094423.
- [29] M. Katsnelson, V. Y. Irkhin, L. Chioncel, A. Lichtenstein, R. A. de Groot, Half-metallic ferromagnets: From band structure to many-body effects, *Rev. Mod. Phys.* 80 (2008) 315.
- [30] L. Chioncel, Y. Sakuraba, E. Arrigoni, M. Katsnelson, M. Oogane, Y. Ando, T. Miyazaki, E. Burzo, A. Lichtenstein, Nonquasiparticle states in Co_2MnSi evidenced through magnetic tunnel junction spectroscopy measurements, *Phys. Rev. Lett.* 100 (2008) 086402.
- [31] S. Fujii, S. Sugimura, S. Asano, et al., Hyperfine fields and electronic structures of the heusler alloys Co_2MnX ($x = \text{Al, Ga, Si, Ge, Sn}$), *J. Phys.: Condens. Matter* 2 (1990) 8583.

- [32] P. Webster, Magnetic and chemical order in heusler alloys containing cobalt and manganese, *J. Phys. Chem. Solids* 32 (1971) 1221–1231.
- [33] P. Brown, K. Neumann, P. Webster, K. Ziebeck, The magnetization distributions in some heusler alloys proposed as half-metallic ferromagnets, *J. Phys.: Condens. Matter* 12 (2000) 1827.
- [34] S. Cheng, B. Nadgomy, K. Bussmann, E. Carpenter, B. Das, G. Trotter, M. Raphael, V. Harris, Growth and magnetic properties of single crystal Co_2MnSi ($x = \text{Si, Ge}$) heusler alloys, *IEEE Trans. Magn.* 37 (2001) 2176–2178.
- [35] B. Ravel, M. Raphael, V. Harris, Q. Huang, Exafs and neutron diffraction study of the heusler alloy Co_2MnSi , *Phys. Rev. B* 65 (2002) 184431.
- [36] M. Raphael, B. Ravel, Q. Huang, M. Willard, S. Cheng, B. Das, R. Stroud, K. Bussmann, J. Claassen, V. Harris, Presence of antisite disorder and its characterization in the predicted half-metal Co_2MnSi , *Phys. Rev. B* 66 (2002) 104429.
- [37] L. Ritchie, G. Xiao, Y. Ji, T. Chen, C. Chien, M. Zhang, J. Chen, Z. Liu, G. Wu, X. Zhang, Magnetic, structural, and transport properties of the heusler alloys Co_2MnSi and NiMnSb , *Phys. Rev. B* 68 (2003) 104430.
- [38] Y. Sakuraba, J. Nakata, M. Oogane, H. Kubota, Y. Ando, A. Sakuma, T. Miyazaki, Huge spin-polarization of 121-ordered Co_2MnSi epitaxial heusler alloy film, *Jpn. J. Appl. Phys.* 44 (2005) L1100.
- [39] L. J. Singh, Z. H. Barber, Y. Miyoshi, Y. Bugoslavsky, W. Branford, L. Cohen, Structural, magnetic, and transport properties of thin films of the heusler alloy Co_2MnSi , *Appl. Phys. Lett.* 84 (2004) 2367–2369.
- [40] W. Wang, M. Przybylski, W. Kuch, L. Chelaru, J. Wang, Y. Lu, J. Barthel, H. Meyerheim, J. Kirschner, Magnetic properties and spin polarization of Co_2MnSi heusler alloy thin films epitaxially grown on $\text{GaAs}(001)$, *Phys. Rev. B* 71 (2005) 144416.
- [41] T. Akiho, J. Shan, H.-x. Liu, K.-i. Matsuda, M. Yamamoto, T. Uemura, Electrical injection of spin-polarized electrons and electrical detection of dynamic nuclear polarization using a heusler alloy spin source, *Phys. Rev. B* 87 (2013) 235205.
- [42] M. Jourdan, J. Minár, J. Braun, A. Kronenberg, S. Chadov, B. Balke, A. Gloskovskii, M. Kolbe, H. Elmers, G. Schönhense, et al., Direct observation of half-metallicity in the heusler compound Co_2MnSi , *Nat. Commun.* 5 (2014).
- [43] A. Rath, C. Sivakumar, C. Sun, S. J. Patel, J. S. Jeong, J. Feng, G. Stecklein, P. A. Crowell, C. J. Palmstrøm, W. H. Butler, et al., Reduced interface spin polarization by antiferromagnetically coupled Mn segregated to the $\text{Co}_2\text{MnSi}/\text{GaAs}(001)$ interface, *Phys. Rev. B* 97 (2018) 045304.

- [44] K. Moges, Y. Honda, H.-x. Liu, T. Uemura, M. Yamamoto, Y. Miura, M. Shirai, Enhanced half-metallicity of off-stoichiometric quaternary heusler alloy $\text{Co}_2(\text{Mn, Fe})\text{Si}$ investigated through saturation magnetization and tunneling magnetoresistance, *Phys. Rev. B* 93 (2016) 134403.
- [45] D. Bombor, C. G. Blum, O. Volkonskiy, S. Rodan, S. Wurmehl, C. Hess, B. Büchner, Half-metallic ferromagnetism with unexpectedly small spin splitting in the heusler compound Co_2FeSi , *Phys. Rev. Lett.* 110 (2013) 066601.
- [46] N. Manyala, Y. Sidis, J. DiTusa, G. Aeppli, D. Young, Z. Fisk, Magnetoresistance from quantum interference effects in ferromagnets, *Nature* 404 (2000) 581.
- [47] S. M. Watts, S. Wirth, S. Von Molnar, A. Barry, J. Coey, Evidence for two-band magnetotransport in half-metallic chromium dioxide, *Phys. Rev. B* 61 (2000) 9621.
- [48] J. Coey, M. Venkatesan, Half-metallic ferromagnetism: Example of CrO_2 , *J. Appl. Phys.* 91 (2002) 8345–8350.
- [49] J. Rodríguez-Carvajal, Fullprof: a program for rietveld refinement and pattern matching analysis, in: satellite meeting on powder diffraction of the XV congress of the IUCr, volume 127, Toulouse, France:[sn], 1990.
- [50] J. Rodríguez-Carvajal, Recent developments of the program fullprof, Commission on powder diffraction (IUCr). *Newsletter* 26 (2001) 12–19.
- [51] J. Rodríguez-Carvajal, Fullprof. 2k, Computer program, Version (2011).
- [52] A. Wills, A new protocol for the determination of magnetic structures using simulated annealing and representational analysis (sarah), *Physica B* 276 (2000) 680–681.
- [53] J. F. Britten, W. Guan, *IUCr Commun. Cryst. Comput., Newsl.* 8 (2007) 96.
- [54] G. M. Sheldrick, *Shelxs 97*, program for the solution of crystal structure, 1997.
- [55] G. Kresse, J. Hafner, Ab initio molecular dynamics for liquid metals, *Phys. Rev. B* 47 (1993) 558.
- [56] G. Kresse, J. Furthmüller, Efficient iterative schemes for ab initio total-energy calculations using a plane-wave basis set, *Phys. Rev. B* 54 (1996) 11169.
- [57] J. P. Perdew, K. Burke, M. Ernzerhof, Generalized gradient approximation made simple, *Phys. Rev. Lett.* 77 (1996) 3865.
- [58] G. Kresse, D. Joubert, From ultrasoft pseudopotentials to the projector augmented-wave method, *Phys. Rev. B* 59 (1999) 1758.
- [59] S. Dudarev, G. Botton, S. Savrasov, C. Humphreys, A. Sutton, Electron-energy-loss spectra and the structural stability of nickel oxide: An *lsda+u* study, *Phys. Rev. B* 57 (1998) 1505.

- [60] H. C. Kandpal, G. H. Fecher, C. Felser, Calculated electronic and magnetic properties of the half-metallic, transition metal based heusler compounds, *J. Phys. D: Appl. Phys.* 40 (2007) 1507.
- [61] A. V. Krukau, O. A. Vydrov, A. F. Izmaylov, G. E. Scuseria, Influence of the exchange screening parameter on the performance of screened hybrid functionals, *J. Chem. Phys.* 125 (2006) 224106.
- [62] E. Gladyshevskii, P. Kripyakevich, M. Y. Teslyuk, O. t. Zarechnyuk, Y. B. Kuzma, Crystal structures of some intermetallic compounds, *Sov. Phys.-Crystallogr* 6 (1961) 207–208.
- [63] R. Sobczak, Magnetische messungen an heusler-phasen Co_2X , *Monatsh. Chem.* 107 (1976) 977–983.
- [64] K. Buschow, P. Van Engen, R. Jongebreur, Magneto-optical properties of metallic ferromagnetic materials, *J. Magn. Magn. Mater.* 38 (1983) 1–22.
- [65] H. Ido, S. Yasuda, Magnetic properties of co-heusler and related mixed alloys, *J. Phys. Colloq.* 49 (1988) C8–141.
- [66] S. Fujii, S. Ishida, S. Asano, Electronic and magnetic properties of $xMn_{1-x}V_xSi$ ($x = Fe$ and Co), *J. Phys. Soc. Jpn.* 63 (1994) 1881–1888.
- [67] G. Bergerhoff, I. Brown, Inorganic crystal structure database (1987).
- [68] Y. Liu, F. Sommer, E. Mittemeijer, Calibration of the differential dilatometric measurement signal upon heating and cooling; thermal expansion of pure iron, *Thermochim. Acta* 413 (2004) 215–225.
- [69] G. Mohapatra, F. Sommer, E. Mittemeijer, Calibration of a quenching and deformation differential dilatometer upon heating and cooling: Thermal expansion of Fe and Fe–Ni alloys, *Thermochim. Acta* 453 (2007) 31–41.
- [70] G. Mohapatra, F. Sommer, E. Mittemeijer, The austenite to ferrite transformation of Fe–Ni under the influence of a uniaxially applied tensile stress, *Acta Mater.* 55 (2007) 4359–4368.
- [71] A. Verma, M. Sundararaman, J. Singh, S. Nalawade, A new method for determining the Curie temperature using a dilatometer, *Meas. Sci. Technol.* 21 (2010) 105106.
- [72] I. Campbell, A. Fert, *Ferromagnetic materials*, EP Wolfarth, North Holland, Amsterdam (1982).
- [73] D. Goodings, Electrical resistivity of ferromagnetic metals at low temperatures, *Phys. Rev.* 132 (1963) 542.
- [74] A. Barry, J. Coey, L. Ranno, K. Ounadjela, Evidence for a gap in the excitation spectrum of CrO_2 , *J. Appl. Phys.* 83 (1998) 7166–7168.

- [75] M. Ito, T. Furuta, K. Kai, A. Taira, K. Onda, I. Shigeta, M. Hiroi, Thermodynamic properties of heusler $\text{Fe}_2\text{-xCo}_x\text{MnSi}$, *J. Magn. Magn. Mater.* 428 (2017) 390–393.
- [76] É. du Trémolet de Lacheisserie, D. Gignoux, M. Schlenker, *Magnetic Resistivity Magnetoresistance, and the Hall Effect*, Springer New York, New York, NY, 2002, pp. 443–460.